European Research Area for Climate Services

ECLISEA

European advances on CLImate Services for Coasts and SEAs

Sectorial Coastal Climate Indicators

Work Package 4- Deliverable D4.C

Author: *Marta Ramírez Pérez, Melisa Menéndez*

***Deliverable Leade**r: UC-IHC*
Participants: *UC-IHC*
Relevant WP: WP4
WP Leader: BRGM

Project acronym: *ECLISEA*
Funding scheme: *ERA4CS Joint Call on Researching and Advancing Climate Services Development by Institutional integration (Topic B)*
Date of the first version deliverable: *April 10, 2021*
Date of final version: *April 24, 2021*

Project ECLISEA is part of ERA4CS, an ERA-NET initiated by JPI Climate, and funded by UC-IHCantabria, HZG, BRGM, NCSRD and CNRS with co-funding by the European Union.

TABLE OF CONTENTS

TABLE OF FIGURES

1. Foreword

ECLISEA is a project that aims to advance coastal and marine climate science and associated services through developing innovative research of sea surface dynamics. To achieve the objectives, ECLISEA is structured in 6 Work-packages (WPs) and this report is associated to the deliverable 4.C of the ECLISEA project. This work-package focuses on the analysis of the Climate Change impact on the most important socio-economic sectors in coastal areas, which are navigation, insurance, energy and tourism. This deliverable aims to develop a database with the sectorial coastal climate indicators along the European coastline and seas for the abovementioned socio-economic sectors. These indicators will be included in the viewer developed in the WP5 (https://ecliseadev.ihcantabria.com/).

The surface dynamics drivers causing the major impacts in coastal areas for the considered sectors are waves, sea level (including the storm surge, the astronomical tide and the mean sea level rise) and wind. The information about these drivers is taken from the datasets presented in the deliverable D3.E and is used to calculate specific indicators at present and future climate conditions under two different climate scenarios. These indicators have been selected by considering the stakeholders needs and based on a literature review.

Thereby, a total of 15 climate impact indicators are defined and their projected changes are evaluated along the European coastline, by comparing historical and future climate conditions. This may help the key climate-sensitive sectors to plan for the future and to develop effective adaptation strategies.

The report is structured as follow: a description of the input data and methods are described in Section 2. The most important impacts affecting the socio-economic sectors and the definition of the considered climate impact indicators are presented in Section 3. Finally, section 4 presents the obtained results in terms of the projected future changes in these indicators.

2. Data and Methods

2.1 Data

2.1.1 *Surface dynamics data*

The Climate Change indicators for the different coastal and marine sectors depend on the most relevant surface dynamics variables causing impacts. These variables include the waves, the storm surge, the mean sea level, the astronomical tide and the wind speed. Information about these variables at the present and future climate conditions are derived from the Regional (RCM) and Global (GCM) Climate Models belonging to the Coupled Model Intercomparison Project Phase 5 (CMIP5). Two different climate scenarios have been also considered, which represent a medium stabilization (RCP4.5) and a high baseline emission (RCP8.5) scenarios. The climate models feed waves and circulation numerical models to obtain waves and sea level variables at regional scale with high spatial resolution (known as dynamical downscaling). A description of the data sources and characteristics used in this report is provided below and is summarized in Table 1. More detailed information about these datasets can be found in WP3.

Table 1. Characteristics of the employed surface dynamics datasets.

Surface dynamics Variable	Dataset name	Domain	Geographical coverage		Spatial resolution	Time periods	Time resolution	Future scenarios
			Latitude interval	Longitude interval				
Waves	UC-IHC	Europe	[23,61]	[-35,17.5]	From 0.08º to 0.5º	1986-2005 2081-2100	hourly	Rcp 4.5 Rcp 8.5
Storm surge	UC-IHC	Southern Europe	[25,46.75]	[-19.9,37.33]	0.08ºx0.06º	1986-2005 2081-2100	hourly	Rcp 4.5 Rcp 8.5
	Copernicus (Muis et al., 2020)	Europe	[9, 88]	[-98, 45]	0.1ºx0.1º	1986-2005 2070-2100	10 - minutes	Rcp 4.5
Mean sea level rise	IPCC (2013)	Global	[-180,180]	[-180,180]	1ºx1º	2007-2100	annual	Rcp 4.5 Rcp 8.5
Astronomical tide	TPX09	Global	[-180,180]	[-180,180]	0.16ºx0.16º	1986-2100	hourly	-
Wind speed	EURO-CORDEX	Europe	[29, 64]	[-11, 42]	0.11ºx0.11º	1986-2005 2081-2100	6-hourly	Rcp 8.5

2.1.1.1 Waves: this study uses the waves climate change projections developed by IHCantabria (UC-IHC) in Europe. This dataset comprises 6 GCMs and 5 RCMs members covering the Atlantic and the Mediterranean domains, respectively. Waves information for the historical period 1986-2005 and for the future period 2081-2100 under two climate scenarios (RCP4.5 and RCP8.5) are available. The spatial resolution varies from 0.08ºx0.08º (along the Spanish Mediterranean coast) to 0.5ºx0.5º in the north of Europe, whereas the temporal resolution is 1-hour.

2.1.1.2 Storm surge: this study uses two different storm surge climate change projections datasets. On one hand, the dataset developed by IHCantabria (UC-IHC) for Southern Europe, which comprises 6 GCMs and 5 RCMs members covering the Atlantic and the Mediterranean domains, respectively. Storm surge information for the historical period 1986-2005 and for the future period 2081-2100 under two climate scenarios (RCP4.5 and RCP8.5) are available. It has an hourly temporal resolution, whereas the spatial resolution is 0.08ºx 0.06º. On the other hand, the dynamical projections of storm surge developed by Muis et al. (2020) for Europe are also considered, which have been generated using the Deltares Global Tide and Surge Model (GTSM) version 3.0. This data are available at Copernicus Climate Change Service (https://climate.copernicus.eu/european-storm-surges). The dataset comprises the storm surge projection of one EURO-CORDEX RCM (the HIRHAM5 model), covering the future period from 2070-2100 under the climate scenario RCP4.5. The spatial and temporal resolution of this dataset is 0.1º along the European coast and 10-minutes, respectively.

2.1.1.3 Sea level rise: the mean sea level rise projections used in the IPCC (2013) are also employed in this study. It comprises data from 21 different GCMs, covering the time period from 2007 to 2100 under two climate scenarios (RCP4.5 and RCP8.5). This dataset has a global coverage (spatial resolution of 1ºx1º) with an annual temporal resolution.

2.1.1.4 Astronomical tide: the hourly time series of astronomical tide is reconstructed for the 21th century based on 13 harmonic constituents from the TPX09 model (Egbert and Erofeeva, 2002). The spatial resolution of this model is 0.16º.

2.1.1.5 Wind speed: we use the wind Climate Change projections from 6 EURO-CORDEX RCMs for the scenario RCP8.5. These RCMs cover Europe with a spatial resolution of 0.11ºx0.11º. They have 6-hourly temporal resolution. We focus on the historical period 1986- 2005 and the future period 2081-2100.

2.1.2 ***Study points***

The Climate Change impact indicators are evaluated along the European coastline. With this purpose, a total of 972 points with a spatial resolution of 0.5º have been defined, which cover from Canary Islands to the Norwegian coast, including the Mediterranean and the Baltic Seas (Figure 2). The depth at these points vary from 5 m to >4000 m. At these study points, information about the surface dynamics at present and future climate conditions is obtained and used to calculate the impact indicators. In addition, some of the impact indicators require information about the nearshore slope, which is taken from Athanasiou et al. (2019) database. These slope values have been capped to $3.33 \cdot 10^{-3}$ (Vousdoukas et al., 2020) (Figure 1).

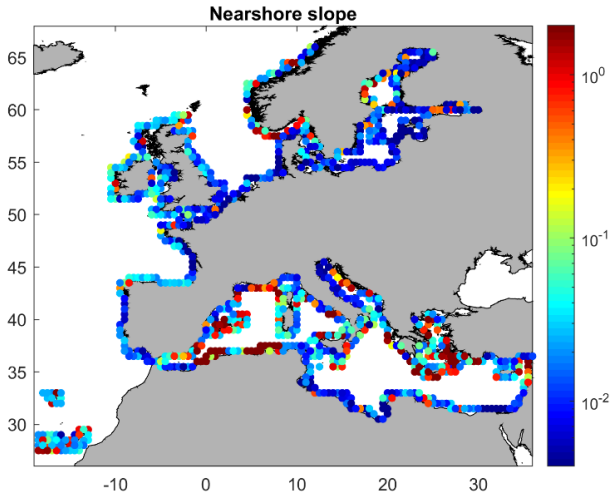

Figure 1. Nearshore slope values at the study points obtained from Athanasiou et al. (2019).

2.2 Methods

2.2.1 *Obtaining surface dynamics at the study points*

The surface dynamics data required to calculate the Climate Change impact indicators at the study points are taken from the nearest nodes of the different datasets.

Most of the indicators that account for the wave conditions, require this information close to the coast instead of in deep-waters as provided by the climate models. As waves approach the shore and the depth decreases, they are affected by the processes of refraction and shoaling. In order to account for these processes, this study applies the Snell's Law to propagate the wave height and direction from deep-waters to a specific shallower depth. The Snell's Law is a simple and computationally efficient method for wave refraction and shoaling assuming straight and parallel bathymetry (Airy, 1845). The propagation depth should be shallow enough to produce the interaction of waves with the bottom but not so much to avoid the wave breaking. For this reason and taken into account the width of the continental shelf along the European coastline, the propagation depth is established in 15 m for the Spanish Atlantic and Norwegian coasts, Ireland and north of Great Britain, whereas for the rest of Europe, this depth is 10 m as shown in Figure 2.

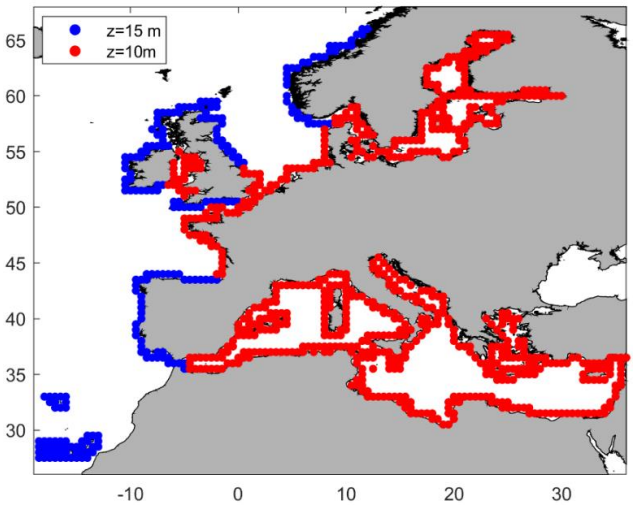

Figure 2. Propagation depth selected for the different coastal points along Europe.

It is important to mention that for the navigation and port-specific indicators, waves are propagated to 10 m regardless the location, which is a reasonable port mouth depth of a medium size harbour.

2.2.2 *Estimation of future changes in climate indicators*

The interest of this report relies on determining the future changes in the most relevant impact indicators of the analyzed sectors. With this purpose, these indicators are calculated for both, the historical (1986-2005) and the future (2081-2100) periods and for both climate scenarios (RCP4.5 and RCP8.5) of all the available climate models (i.e. members). Then, the anomaly with respect to the baseline climate of the same model (GCM/RCM) is computed. Finally, the multi-model ensemble of these future changes is derived by computing the arithmetic mean of the individual members anomalies. Differences with respect to the recent past conditions (i.e., historical period) are expressed in absolute and/or in relative (%) values. The significance of the change is determined according to the following condition: the change is considered significant when the multi-model ensemble mean exceeds the inter-model standard deviation (Hemer et al., 2013).

3. The climate impact indicators

3.1 Selection of indicators according to stakeholders needs

This section describes the most important climate impacts affecting the considered socio-economic sectors and the corresponding indicator used to assess that impact. The selected indicators are commonly used for this kind of studies and therefore are widely accepted by the scientific community. Figure 3 shows the indicators defined for each sector and the corresponding assessed impact.

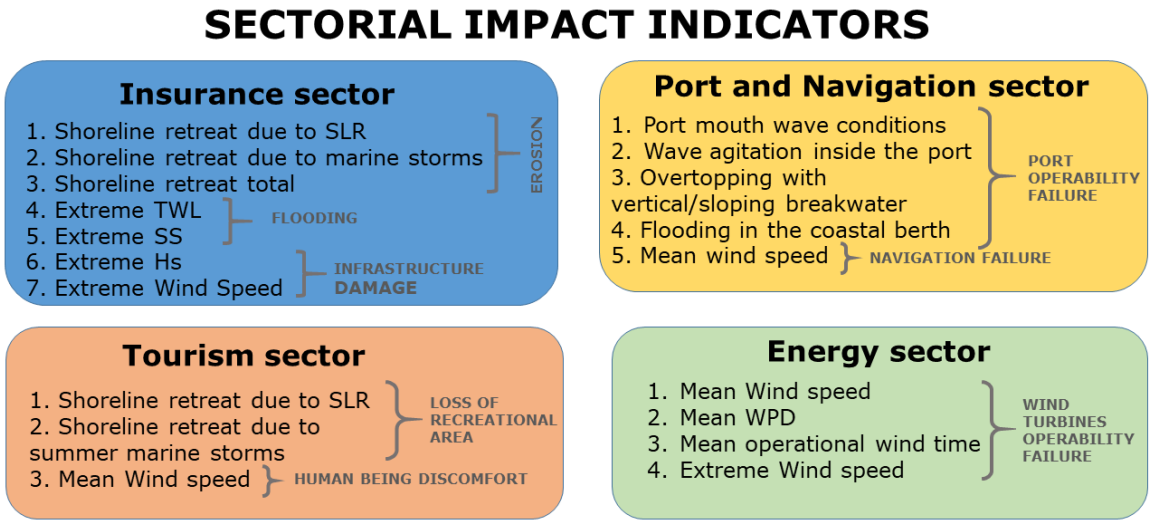

Figure 3. Impact indicators selected for each socio-economic sector. The corresponding coastal impact is also specified.

3.1.1 *Insurance sector:*

The most important Climate Change impacts affecting the socio-economic sector of insurance in coastal areas are the coastal flooding and erosion as well as the infrastructure damages. To characterize these impacts, 7 different indicators have been selected: the shoreline retreat due to mean sea level rise, to marine storms and to the combination of both; and the extreme conditions in total water level (TWL), significant wave height (Hs), storm surge (SS) and wind speed, which are characterized based on the 50 years return value. While the shoreline retreat indicators account for the erosion impact, the extreme TWL and extreme SS produce coastal flooding. Finally, the extreme Hs and wind speed are responsible for coastal infrastructure damages.

3.1.2 *Tourism sector:*

The tourism in coastal areas focuses on relaxing on the beaches and performing other activities connected with the sea. For this reason, the loss of recreational area and the human beings discomfort due to atmospheric conditions are the most relevant threads identified for this sector. These impacts are considered in this study through the evaluation of the shoreline retreat due to mean sea level rise and due to summer marine storms and through the changes in mean wind speed.

3.1.3 *Port and Navigation sector:*

The knowledge of extremes wave climate and wind speed is of outstanding importance for the navigation and the proper port operation. Changes in the incident wave conditions affect the agitation inside the port, the overtopping breakwaters and the coastal flooding at the berth frequencies. Meanwhile, the navigation is altered by the wave conditions at

the port mouth and by the wind speed. These 5 indicators are used to assess the Climate Change impacts in port and navigation.

3.1.4 *Energy sector:*

The wind turbines operate under specific wind conditions, since weak winds or very intense wind speeds limit their activity. Impacts associated with future variations in the wind speed conditions are evaluated here through the changes in mean and extreme wind speed, the mean wind power density and the mean operational wind time.

3.2 Definition of climate impact indicators

This section includes a detailed description of the 15 considered climate impact indicators. In particular, the definition, the assumptions, the equations as well as the input and output data for estimating the different indicators are presented. A summary of these indicators and the magnitude of the projected future change (in terms of absolute or relative values) are provided in Table 2.

Nº	Impact indicator	Impact	Sector	Result
1	Shoreline retreat due to SLR	Erosion; loss of recreational area	Insurance, Tourism	Absolute change (m)
2	Shoreline retreat due to marine storms	Erosion	Insurance	Absolute change (%)
3	Shoreline retreat due to summer marine storms	Loss of recreational area	Tourism	Absolute change (%)
4	Total shoreline retreat (SLR+storms)	Erosion	Insurance	Absolute change (m)
5	Extreme Total Water Level	Flooding	Insurance	Absolute (m) and Relative change (%)
6	Extreme Significant Wave Height	Infrastructure damage	Insurance	Relative change (%)
7	Extreme Storm Surge	Flooding	Insurance	Relative change (%)
8	Unfavorable port mouth wave conditions	Port operability failure	Navigation	Absolute change (hours/year)
9	Surface agitation inside the port		Navigation, Tourism	Absolute change (hours/year)
10	Coastal Flooding at the berth	Port operability failure; Infrastructure damage	Navigation	Absolute change (hours/year)
11	Wave overtopping for vertical/sloping breakwater		Navigation	Absolute change (hours/year)
12	Mean Wind Speed	Human being discomfort; wind turbines operability failure; navigation failure.	Tourism, Energy, Navigation	Relative change (%)
13	Mean Wind Power Density	Wind turbines operability failure	Energy	Relative change (%)
14	Mean Operation Wind Time		Energy	Relative change (%)
15	Extreme Wind Speed	Infrastructure damage; wind turbines operability failure	Energy	Relative change (%)

2. Sectorial impact indicators.

3.2.1 *Changes in Shoreline Retreat induced by Sea-Level Rise*

- Definition: this indicator is based on the Bruun rule (Bruun, 1962; Bruun, 1988), with the underlying assumptions of considering that sediment transport only occurs perpendicularly to the shoreline. Thus, any tri-dimensional variability is neglected and it is assumed that the coastal profile is an equilibrium profile with uniform sediment size.
- Equation:

$$\Delta S = \frac{\Delta RSLC}{\tan(\beta)}$$

  Where ΔS is the shoreline retreat due to mean sea level rise at a given year horizon, $\Delta RSLC$ is the relative mean sea level rise (in meters) and $\tan(\beta)$ is the nearshore slope.
- Units: meters (positive values indicate shoreline retreat).
- Inputs: the regional sea-level change (in m) and the slope of the active profile (from the depth of closure to the top of the upper shoreface). The regional sea-level change data in Europe is derived from the IPCC (2013) database, whereas the nearshore slope is obtained from Athanasiou et al. (2019).
- Output: the shoreline retreat due to Sea-level Rise has been calculated for the year 2100 under both analyzed scenarios (RCP4.5 and RCP8.5).

3.2.2 *Changes in Shoreline Retreat induced by marine storms*

- Assumptions: this indicator is based on the Storm Erosion Index (SEI) proposed by Miller and Livermont (2008). It uses the Peak Erosion Index (PEI) integrated over the duration of the storm, assuming the equilibrium beach profile theory. Storms are defined here as events where the PEI is higher than the 95th percentile. Exceedances separated by less than 48 hrs are considered to be the same event. The SEI are then normalized by the storm duration and the indicator represents the mean value of these SEI.
- Equations:

$$PEI\ (t_i) = W_*(t_i)\left[\frac{0.068 \cdot H_b(t_i) + S(t_i)}{B + 1.28 \cdot H_b(t_i)}\right]$$

$$SEI = \sum_{i=1}^{t_d} PEI(t_i)$$

  Where W_* is the width of the active surfzone; H_b is the depth limited breaking wave height; S is the storm water elevation with respect to mean sea level and B, the local berm height.
- Units: meters (positive values indicate shoreline retreat).
- Inputs: The berm height is assumed constant and equal to 1. The hourly time series of storm surge and waves come from the UC-IHC climate projections dataset. Then, H_b is estimated using the propagation by the Snell's law and the depth-induced constant wave breaking criterion:

$$\frac{H_b}{h_b} = \gamma$$

Where h_b is the wave breaking depth estimated according to Guo (2002) and ɣ is equal to 0.55.

W_* is given by:

$$W_* = \left(\frac{h_b}{A}\right)^{3/2}$$

where h_b is the wave breaking depth and A is the so-called "profile scale parameter" (Dean 1976; Dean 1985). A is calculated as follow:

$$A = d_c \left(\frac{\tan(\beta)}{d_c + B}\right)^{\frac{2}{3}}$$

where tan(β) is the nearshore slope obtained from Athanasiou et al. (2019), B is the berm height and dc is the depth of closure, estimated based on Hinton and Nicholls (1998):

$$dc = 2.28 \cdot H_{12} - 68.5 \cdot \left(\frac{H_{12}^2}{gT^2}\right)$$

where Hs_{12} is the non-breaking significant wave height that is exceeded for 12 h per year, T is the associated wave peak period and g is the acceleration due to gravity.

- Output: the mean shoreline retreat due to marine storms has been calculated for the historical period 1986-2005 and for the future period 2081-2100 under both analyzed scenarios (RCP4.5 and RCP8.5). Then, the magnitude of the future changes has been determined.

3.2.3 *Changes in Shoreline Retreat induced by summer marine storms*

This indicator is calculated following the same approach as described in 3.2.2 but considering uniquely the time series of waves and storm surge during the summer season (i.e. the months of June, July and August).

3.2.4 *Changes in total Shoreline Retreat (SLR + marine storms)*

- Definition: the total shoreline retreat (ΔS_T) combines the effect of the two major drivers: the mean sea level rise and the marine storms. Since the available Climate Models for both dynamics are different, this indicator is calculated by adding the mean ensemble of the individual shoreline retreat changes (ΔS_{SLR} and ΔS_{storms}, respectively).
- Equation:

$$\Delta S_T = \Delta S_{SLR} + \Delta S_{storms}$$

- Units: meters (positive values indicate shoreline retreat).
- Input data: the 20-years mean (from 2081 to 2100) shoreline retreat changes due to sea level rise and due to marine storms respect to the historical period 1986-2005, under both climate scenarios (RCP4.5 and RCP8.5).
- Output data: the magnitude of the future changes in the total shoreline retreat (in meters).

3.2.5 *Changes in coastal extreme Total Water Level*

- Definition: the Total Water Level (TWL) is the combination of tides, surge and wave run-up. The extreme values of this parameter is characterized here by the TWL of 50 years return period, which is estimated by fitting a Gumbel distribution based on the annual maxima (see this function in 3.2.6).
- Equation:

$$TWL\,(t_i) = S(t_i) + AT + SLR(t_i) + R_2(t_i)$$

  Where S is the storm surge, AT is the astronomical tide, SLR is the sea level rise and R_2 is the wave runup ($R_{2\%}$).
- Units: meters (m) and percentage (%).
- Inputs: The hourly time series of storm surge and waves come from the UC-IHC climate projections dataset. The Regional sea-level rise data are obtained from the IPCC (2013) database. Finally, the astronomical tide in represented by the average monthly highest astronomical tide derived from the global tide model TPXO9. Based on the wave parameters, the wave runup is calculated according to Stockdon et al. (2006):

$$R_{2\%} = 1.1 \cdot \left(0.35\beta_f (H_0 L_0)^{1/2} + \frac{\left[H_0 L_0 (0.563\beta_f^2 + 0.004)\right]^{1/2}}{2} \right)$$

  Where H_0 is the significant wave height at 10 m or 15 m depth (see Figure 2) propagated from deep waters using the Snell's Law. The deep water peak wave wavelength, L_0, is derived from:

$$L_0 = \frac{g \cdot T_p^2}{2\pi}$$

  Where T_p is the wave peak period and g, the acceleration due to gravity.

  Finally, β_f is the foreshore beach slope, which is determined here according to Melet et al. (2020). The equation used to estimate this parameter is that proposed by Sunamura (1984), since this formulation lets the beach slope evolve with varying incoming wave conditions:

$$\beta_f = 0.12 \cdot \left[\frac{\sqrt{2\pi D_{50} L_p}}{H_s} \right]^{1/2}$$

  Where H_s is the propagated significant wave height at 10 m or 15 m depth and L_p is the deep water peak wave wavelength calculated based on the wave peak period. D_{50} is the median diameter of the beach sand, which is assumed equal to 250 µm (for fine to medium-grained sand size) (Rueda et al., 2017). The resulting time series of β_f are then capped at 0.2 and scaled by normalization factor to ensure that the time mean of the beach slope stays close to 0.04 (Melet et al., 2020).
- Output: the absolute and relative changes in the extreme (50-years return period) TWL from 2081-2100 with respect to the 50-yr TWL from 1986-2005 under both analyzed scenarios (RCP4.5 and RCP8.5).

3.2.6 *Changes in extreme Significant Wave Height*

- Definition: The extreme values of this parameter are characterized here by the Significant Wave Height (Hs) of 50 years return period, which is estimated by fitting a Gumbel distribution based on the annual maxima.
- Equation:

$$XT = \beta - \alpha \ln\left[-\ln\left(1 - \frac{1}{TR}\right)\right]$$

  This equation corresponds to an extreme value type I distribution (i.e. Gumbel distribution), where α and β are the scale and location parameters and Tr is the return period (50 years in this case).
- Units: percentage (%).
- Inputs: we use the hourly time series of deep-water Hs derived from the UC-IHC Climate Change projections dataset.
- Output: the relative changes in the extreme (50-years return period) Hs from 2081-2100 with respect to the 50-yr Hs from 1986-2005 under both analyzed scenarios (RCP4.5 and RCP8.5).

3.2.7 *Changes in extreme Storm Surge*

- Definition: The extreme values of this parameter are characterized here by the Storm Surge (SS) of 50 years return period, which is estimated by fitting a Gumbel distribution based on the annual maxima.
- Equation:

$$XT = \beta - \alpha \ln\left[-\ln\left(1 - \frac{1}{TR}\right)\right]$$

  This equation corresponds to an extreme value type I distribution (i.e. Gumbel distribution), where α and β are the scale and location parameters and Tr is the return period (50 years in this case).
- Units: percentage (%).
- Inputs:, we use the hourly time series of storm surge derived from the UC-IHC climate projections dataset and the 10-minutes time series from Muis et al. (2020).
- Output: the relative change in the extreme (50-years return period) SS from 2081-2100 with respect to the 50-yr SS from 1986-2005 under both analyzed scenarios (RCP4.5 and RCP8.5) for the two considered datasets.

3.2.8 *Changes in port operability failure due to unfavorable port mouth conditions*

- Definition: This indicator corresponds to the number of hours per year for which the significant wave height at the port mouth exceeds the threshold of 2.5 m. Under these circumstances, the port cannot operate.
- Units: hours per year.
- Inputs: we use the hourly time series of significant wave height derived from the UC-IHC Climate Change projections dataset. To estimate the significant wave height at the port mouth, deep-waters waves are propagated to 10 m depth using

the Snell's Law and the breaking criterion from Goda (1975) is applied to account for wave breaking.

- Output: based on the hourly time series of 10-m depth Hs, we determine the number of values higher than 2.5 m and we divide by the number of years (i.e. 20) to obtain the number of hours per year. Then, we calculate the changes in the hours per year for which Hs > 2.5 m from 2081-2100 with respect to this number from 1986-2005 under both analyzed scenarios (RCP4.5 and RCP8.5).

3.2.9 *Changes in port operability failure due to surface agitation*

- Definition: This indicator is defined as the number of hours per year for which the diffracted wave height inside the port exceeds the threshold of 0.4 m.
- Units: hours per year.
- Inputs: we use the hourly time series of significant wave height derived from the UC-IHC Climate Change projections dataset. To estimate the significant wave height at the port mouth, deep-waters waves are propagated to 10 m depth using the Snell's Law and the breaking criterion from Goda (1975) is applied to account for wave breaking. Then, we estimate the wave height inside the port by multiplying the wave height propagated to the port mouth by a diffraction coefficient (Izaguirre et al., 2021):

$$H_{InsidePort} = DC \cdot H_{prop}$$

  The assumed diffraction coefficient (DC) corresponds to a very good shelter afforded (DC= 0.15).
- Output: based on the hourly time series of the wave height inside the port, we determine the number of values higher than 0.4 m and we divide by the number of years (i.e. 20) to obtain the number of hours per year. Then, the changes in the hours per year for which $H_{InsidePort}$ > 0.4 m from 2081-2100 with respect to this number from 1986-2005 is calculated under both analyzed scenarios (RCP4.5 and RCP8.5).

3.2.10 *Changes in coastal flooding at the berth*

- Definition: This indicator corresponds to the number of hours per year with coastal flooding at the berth.
- Equation:

$$CF = TWL - (MHT + F)$$

  where CF is the coastal flooding height, TWL is the Total Water Level, MHT is the maximum high tide and F is the freeboard of the berth (Izaguirre et al., 2021). The total water level is calculated as:

$$TWL\,(t_i) = 0.5 \cdot Hs(t_i) + S(t_i) + AT(t_i) + SLR(t_i)$$

  where 0.5·Hs is the wave set-up, S is the storm surge, AT is the astronomical tide and SLR is the sea level rise.
- Units: hours per year.
- Inputs: we use the hourly time series of significant wave height and storm surge derived from the UC-IHC Climate Change projections dataset. To estimate the significant wave height at the port mouth, deep-waters waves are propagated to

10 m depth using the Snell's Law and the wave breaking criterion from Goda (1975) is also applied. The sea-level rise data are obtained from the IPCC (2013) database. The time series of astronomical tide are derived from the global tide model TPXO9. Based on this 20-years time series, the maximum high tide is calculated. Finally, we assume a freeboard in the berth of 1 m.

- Output: Once we have calculated the hourly CF time series, we determine the number of values higher than 0 m and we divide by the number of years (i.e. 20) to obtain the number of hours per year. Then, we derive the changes in the hours per year with CF from 2081-2100 with respect to this number from 1986-2005 under both analyzed scenarios (RCP4.5 and RCP8.5).

3.2.11 *Changes in wave overtopping conditions for vertical/sloping breakwaters*

- Definition: for wave overtopping considering a vertical breakwater, we use an indicator obtained from the empirical formulation of Franco et al. (1994), whereas for wave overtopping with a sloping breakwater, we use the empirical formulation of Waal and van der Meer (1992). Both formulations have been implemented by Izaguirre et al. (2021) and refer to the number of hours per year with overtopping discharge exceeding the threshold of 0.1 l/s/m.
- Equations:
  - Vertical breakwater:

$$Q = \frac{q}{\sqrt{gH_s^3}} = 0.2e^{\left(-b\frac{R_c}{H_s}\right)}$$

  - Sloping breakwater:

$$Q = \frac{q}{\sqrt{gH_s^3}} = 8 \cdot 10^{-5} \cdot e^{\left(-b\frac{R_c}{H_s}\right)} \cdot e^{(3.5 \cdot b \cdot \vartheta_r)}$$

  where Q is the dimensionless overtopping, q is the overtopping discharge ($m^3/(ms)$), Hs is the significant wave height (m), Rc is the freeboard, b is the coefficient depending on the breakwater typology (b= 4.3 for vertical breakwaters and b=3.1 for sloping breakwaters) and ϑ_r is the reduction coefficient depending on the roughness (ϑ_r=0.55). The freeboard is calculated as:

$$Rc = R - SLR$$

  where R is the breakwater freeboard and SLR is the sea level rise.
- Units: hours per year.
- Inputs: we use the hourly time series of significant wave height derived from the UC-IHC Climate Change projections dataset. To estimate the significant wave height at the port mouth, deep-waters waves are propagated to 10 m depth using the Snell's Law and the wave breaking criterion from Goda (1975) is also applied. The sea-level rise data are obtained from the IPCC (2013) database. The considered breakwater freeboard is 5 m.

- Output: Once we have calculated the hourly q time series, we determine the number of values higher than 0.1 l/m/s and we divide by the number of years (i.e. 20) to obtain the number of hours per year. Then, we estimate the changes in the hours per year with q threshold exceedance from 2081-2100 with respect to this number from 1986-2005 under both analyzed scenarios (RCP4.5 and RCP8.5).

3.2.12 *Changes in mean Wind speed*

- Definition: The wind resource is represented here by the mean wind speed. Furthermore, this indicator is also used to analyze the level of discomfort of tourists on the beach or the stop in navigation due to strong wind conditions.
- Units: percentage (%).
- Inputs: we use the 6-hourly time series of wind speed at 10 meters height provided by the EURO-CORDEX RCMs dataset.
- Output: we calculate the changes in the wind resource as the difference in the mean wind speed from 2081-2100 with respect to 1986-2005 under the most pessimistic climate scenario (i.e., RCP8.5).

3.2.13 *Changes in mean Wind Power Density*

- Definition: The wind power density is a measure of the amount of the wind energy available at any location. Here, we calculate wind power density at 100 m height, which represents the average hub height of the currently operating windfarms within North Sea.
- Equation:

$$WPD = 12 \cdot \rho \cdot W^3$$

Where WPD is the Wind Power Density in W/m^2, ρ is the corrected air density in kg/m^3 and W is the 100-m wind speed in m/s. The air density is corrected to take into account the hub height (HH) influence in reducing the reference value ρ_0=1.225 (Hennessey, 1977):

$$\rho = \rho_0 - 1.194 \cdot 10^{-4} \cdot HH$$

- Units: percentage (%).
- Inputs: we use the 6-hourly time series of wind speed at 10 meters height provided by the EURO-CORDEX RCMs dataset.
- Output: we calculate the changes in the mean wind power density between the future (2081-2100) and the recent past conditions (1986-2005) under the most pessimistic climate scenario (i.e., RCP8.5).

3.2.14 *Changes in mean operational Wind time*

- Definition: The operation wind time provides information about the time in which a wind turbine operates. We assume the typical values of cut in and cut off wind speed for currently operating turbines of 4 m/s and 25 m/s, respectively. The operational wind time (OT) is expressed as percentage of time with operating turbines.
- Equation:

$$OT = \frac{time_{cut\ in-cut\ off}}{time_{total}}$$

- Units: percentage (%).
- Inputs: we use the 6-hourly time series of wind speed at 100 meters height provided by the EURO-CORDEX RCMs dataset.
- Output: we calculate the changes in the mean operational wind time between the future (2081-2100) and the recent past conditions (1986-2005) under the most pessimistic climate scenario (i.e., RCP8.5).

3.2.15 *Changes in Extreme Wind Speed*

- Definition: the extreme wind conditions are represented through the 50 years return value of surface (10-m) wind speed. This extreme value plays an important role in the dimensioning of the turbine support structure and may cause significant coastal infrastructure damages.
- Equation:

$$XT = \beta - \alpha \ln\left[-\ln\left(1 - \frac{1}{TR}\right)\right]$$

  This equation corresponds to an extreme value type I distribution (i.e. Gumbel distribution), where α and β are the scale and location parameters and Tr is the return period (50 years in this case).
- Units: percentage (%).
- Inputs: we use the annual maxima of the 6-hourly time series of 10-m wind speed provided by the EURO-CORDEX RCMs. Based on these maxima, we fit a Gumbel distribution to derive the 50-yr return value.
- Output: we calculate the changes in the 50-yr wind speed in the future period 2081-2100 with respect to the 50-yr wind speed in 1986-2005 under the most pessimistic climate scenario (i.e., RCP8.5).

4. Results

This section presents the most relevant results in terms of the expected future changes in the impact indicators under both analyzed climate scenarios respect to their values at the historical period 1986-2005.

4.1.1 *Changes in Shoreline Retreat induced by Sea-Level Rise*

The changes in the shoreline retreat due to mean sea level rise at the year 2100 oscillate from -138.1 to +154.85 m under the RCP4.5, and from -69.22 to +221.3 m, under the RCP8.5 (positive values indicates shoreline retreat). Negative values are found at the Gulf of Bothnia, in the north of the Baltic Sea, where a future decrease in the mean sea level is expected for both analyzed climate scenarios (Figure 4). The highest increases are observed in the French and North Sea coasts. These results agree with the patterns observed by Thiéblemont et al. (2020).

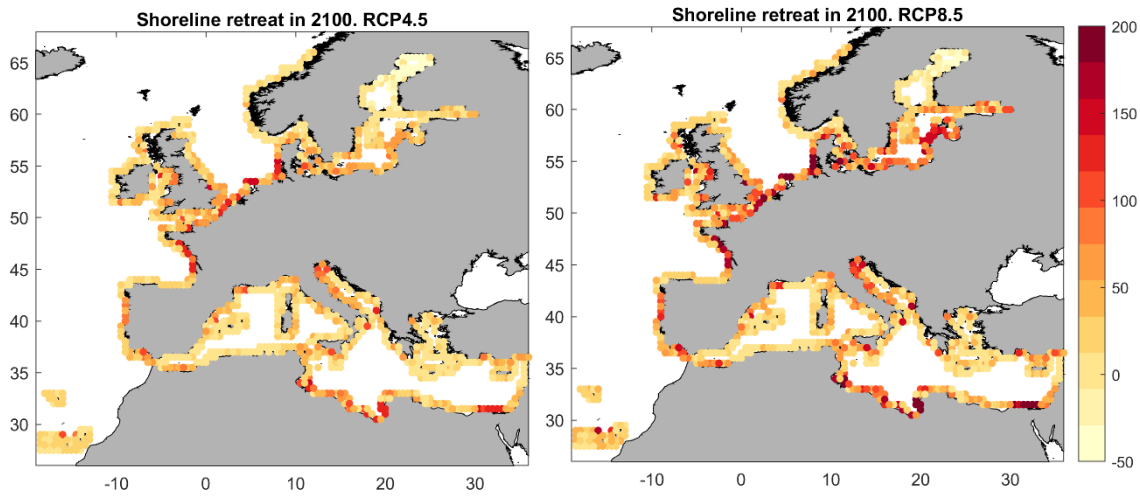

Figure 4. Magnitude of the changes (in meters) in the shoreline retreat due to mean sea level rise in 2100 under (left) the RCP4.5 and (right) RCP8.5 scenarios.

4.1.2 *Changes in Shoreline Retreat induced by marine storms*

This indicator is evaluated along the coasts of Southern Europe, where both waves and storm surge projections for the same Climate Models are available. In this region, the shoreline retreat due to marine storms exhibits values from 0.03 m to 126.5 m for the historical period 1986-2005, with the highest retreats detected in the north of Portugal and southwest of France. These values are expected to diminish in the future period 2081-2100 under both climate scenarios for most of the analyzed area. The most significant decreases (minimum of -7.46 m and -15.21 m for RCP4.5 and RCP8.5, respectively) are observed in the Gulf of Cadiz, north of Portugal, southwest of France, around the Montpellier coasts and north of the Ligurian Sea. A slight increase (maximum of 0.35 and 0.52 m for RCP4.5 and RCP8.5, respectively) is observed in Canary and Madeira islands (Figure 5).

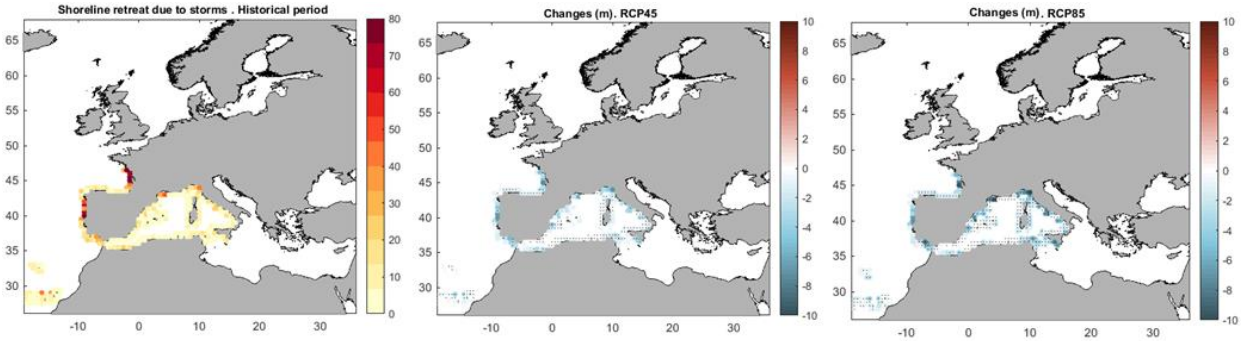

Figure 5. (Left) Historical (1986-2005) shoreline retreat due to marine storms along the coasts of southern Europe. Magnitude of the changes (in meters) for the future period 2081-2100, under (center) RCP4.5 and (right) RCP8.5 climate scenarios. Stippling denotes areas where the magnitude of the multi-model ensemble mean exceeds the inter-model standard deviation.

4.1.3 *Changes in Shoreline Retreat induced by summer marine storms*

As observed in the previous indicator, the maximum values of historical shoreline retreat due to summer marine storms are found in the north of Portugal and southwest of France, followed by the Montpellier coast and north of the Ligurian Sea (with maximum values of 25.03 m). These areas also show the most significant decreases in 2081-2100 (-4.43 m and -6.89 m, for RCP4.5 and RCP8.5, respectively). However, in this case, the observed future changes show specific features such as the increases in the south of the Mediterranean Sea and Canary Islands (with a maximum increase of 1.61 m and 1.58 m, for RCP4.5 and RCP8.5, respectively) (Figure 6).

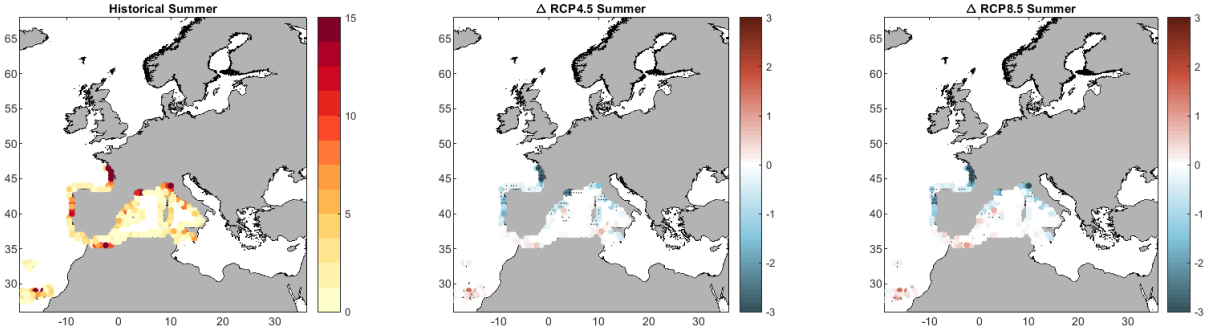

Figure 6. (Left) Historical (1986-2005) shoreline retreat due to summer (JJA) marine storms along the coasts of southern Europe. Magnitude of the changes (in meters) for the future period 2081-2100, under (center) RCP4.5 and (right) RCP8.5 climate scenarios. Stippling denotes areas where the magnitude of the multi-model ensemble mean exceeds the inter-model standard deviation.

4.1.4 *Changes in total Shoreline Retreat (SLR + marine storms)*

The patterns and magnitude of the historical total shoreline retreat coincide with those induced by marine storms, since the SLR at this period is considered zero (values oscillating between 0.03 m and 126.5 m). The future changes (from 2081 to 2100) in this indicator present the highest rises along the Portuguese coast, southwest of France, Gulf of Cadiz and in the Ligurian Sea, with the magnitudes oscillating between -2.47 m to +42.87 m and from -8.72 m to +56.15 m for the RCP4.5 and RCP8.5, respectively. The contribution of the SLR to the total shoreline retreat in 2081- 2100 period is 58% and 65% for RCP4.5 and RCP8.5, whereas these values are 42% and 35% for the marine storms.

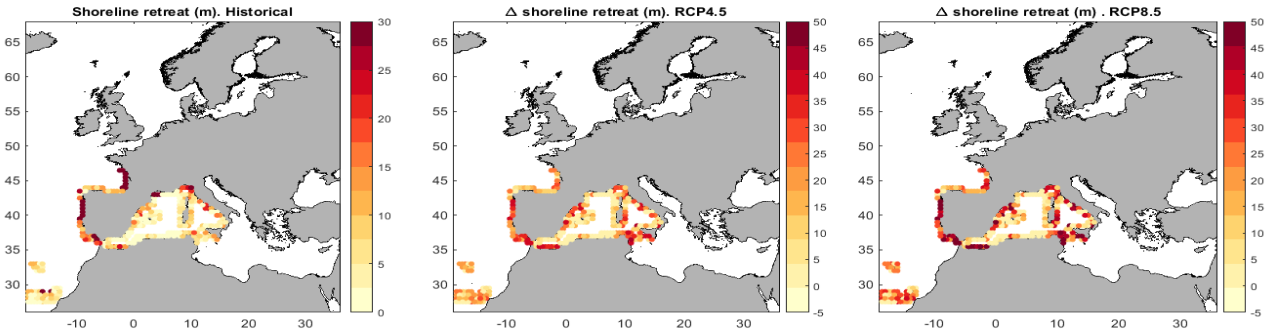

Figure 7. (Left) Historical (1986-2005) total shoreline retreat (SRL + marine storms) along the coasts of southern Europe. Magnitude of the changes (in meters) for the future period 2081-2100, under (center) RCP4.5 and (right) RCP8.5 climate scenarios. Stippling denotes areas where the magnitude of the multi-model ensemble mean exceeds the inter-model standard deviation.

4.1.5 *Changes in coastal extreme Total Water Level*

The coastal extreme total water level (TWL) has been evaluated for Southern Europe by means of the 50 years return value obtained by fitting a Gumbel distribution. The historical values in this indicator vary from 1.25 m to 5.75 m, with magnitudes lower than 2.5 m found the Mediterranean Sea, from 3-4 m in the Canary and Madeira Islands and > 4 m along the Atlantic coast of Spain, Portugal and France. The projected future changes in this indicator for the 2081-2100 period show an increase everywhere, from 0.15-0.66 m and from 0.25-0.91 m for the RCP4.5 and RCP8.5 (Figure 8). In relative terms, these changes correspond to an increase of 2.7-39% and of 7.6-50.88% for both RCPs (

Figure 9). These results agree in both the spatial patterns and the magnitude of the historical and future changes with those obtained by Vousdoukas et al. (2017).

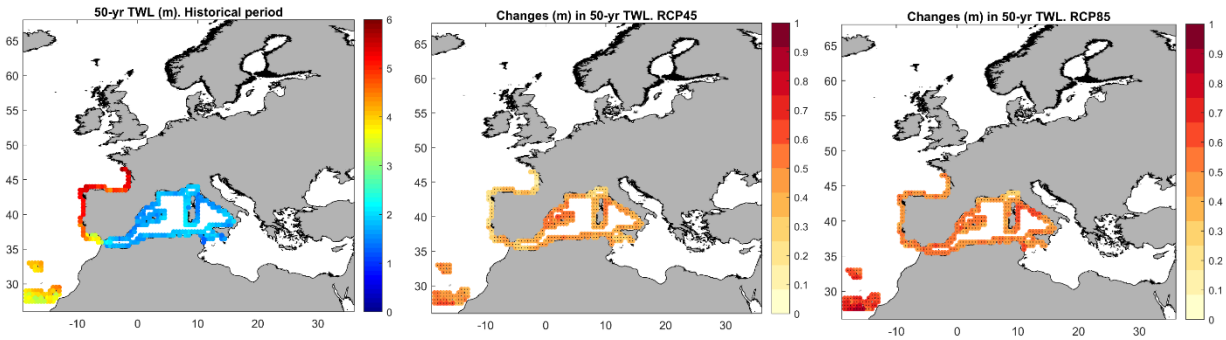

Figure 8. (Left) Historical (1986-2005) extreme TWL (m) in southern Europe. Magnitude of the changes (in meters) for the future period 2081-2100, under (center) RCP4.5 and (right) RCP8.5 climate scenarios. Stippling denotes areas where the magnitude of the multi-model ensemble mean exceeds the inter-model standard deviation.

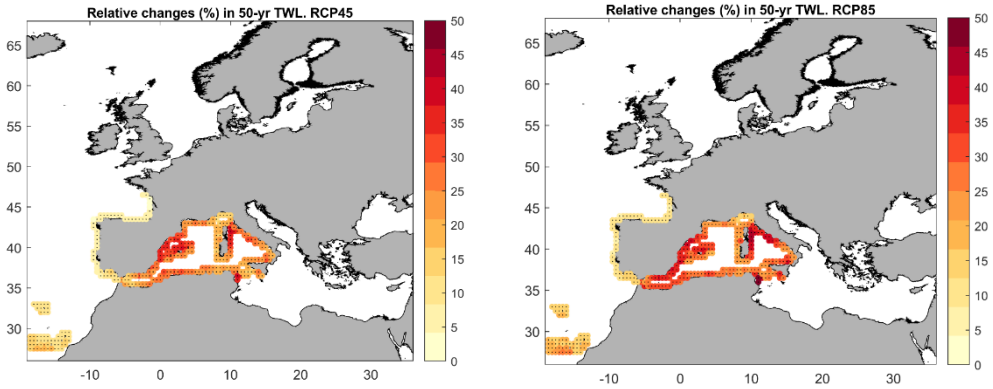

Figure 9. Future changes in the extreme TWL relative to their values in the historical period under (left) RCP4.5 and (right) RCP8.5 climate scenarios. Changes are expressed in percentage (%). Stippling denotes areas where the magnitude of the multi-model ensemble mean exceeds the inter-model standard deviation.

4.1.6 *Changes in extreme Significant Wave Height*

The extreme (50-years return value) significant wave height has been evaluated along the European Atlantic coast and the Western Mediterranean basin. The historical 50-yr Hs exhibits values from 0.74 m to 14.29 m. The projected future changes in this indicator show similar

range of variations for both RCPs, with relative changes from -10.62% to +12.62% and from -10.67% to 11.42% for RCP4.5 and RCP8.5, respectively. However, the spatial patterns observed for both RCPs differ at specific locations and the changes found for the RCP4.5 are more noticeable than for RCP8.5. These special features are also observed by Lobeto et al. (2021) and Meucci et al. (2020), who applied a similar analysis at global scale.

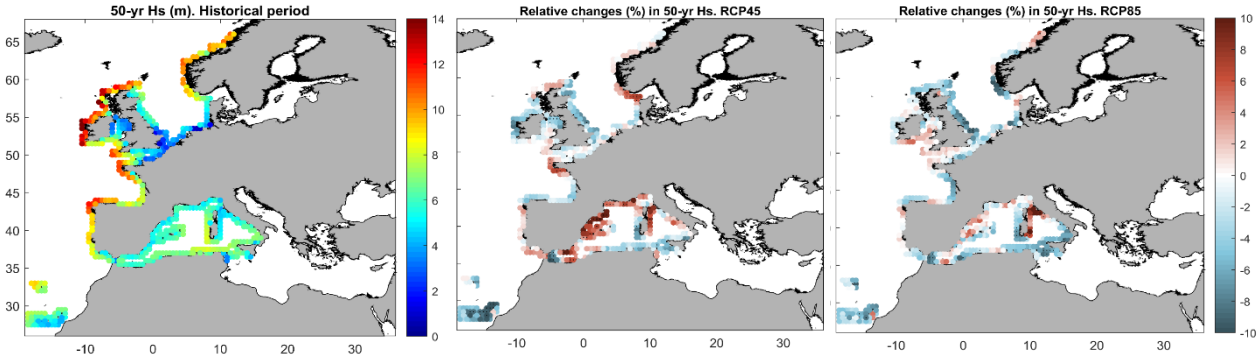

Figure 10. (Left) Historical (1986-2005) extreme Hs (m) variations along the European Atlantic coast and the Western Mediterranean basin. Relative future changes (in percentage) for the future period 2081-2100, under (center) RCP4.5 and (right) RCP8.5 climate scenarios. Stippling denotes areas where the magnitude of the multi-model ensemble mean exceeds the inter-model standard deviation.

4.1.7 *Changes in extreme Storm Surge*

The extreme (50-years return value) storm surge has been evaluated based on two different datasets. On one hand, the mean ensemble of the future changes from 6 GCMs (for the Atlantic coast) and 5 RCMs (for the Mediterranean coast) is calculated for Southern Europe (UC-IHC dataset). On the other hand, the future changes in this indicator obtained by Muis et al. (2020) for one RCM in Europe are also considered. For the first dataset, the historical 50-yr SS exhibits values from 0.13 m to 1.03 m. Similar values are observed for the second dataset except in the Cantabrian Sea and in the north of the Adriatic Sea, where are slightly higher. The relative changes obtained for the UC-IHC dataset show specific spatial patterns, with an increase in the 50-yr SS in the Western Mediterranean and Atlantic coasts and a decrease on the Eastern Mediterranean and Canary Islands under the RCP4.5 (range of variations from -19.9% to +12.36%). These patterns are slightly different under the RCP8.5, where this indicator decreases in the Mediterranean Sea and increases everywhere else (range of variations from -33.66% to +21.64%) (Figure 11). In the case of Muis et al. (2020) SS projections, the future changes in the 50-yr SS for the RCP4.5 are significantly higher, which can be explained by the use of a single climate model (i.e. the EUROCORDEX HIRHAM5) (Figure 12).

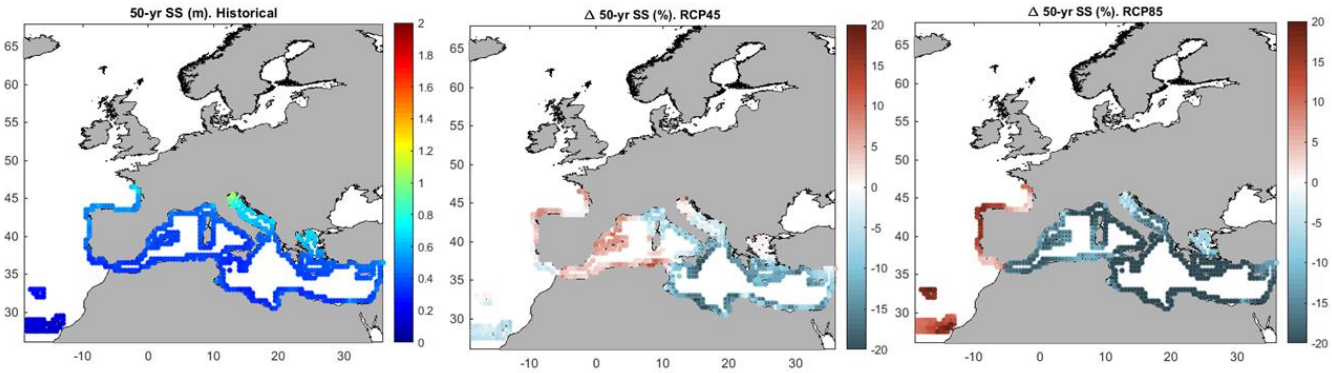

Figure 11. (Left) Historical (1986-2005) extreme storm surge (m) in Southern Europe. Relative future changes (in percentage) for the future period 2081-2100, under (center) RCP4.5 and (right) RCP8.5 climate scenarios. Stippling denotes areas where the magnitude of the multi-model ensemble mean exceeds the inter-model standard deviation.

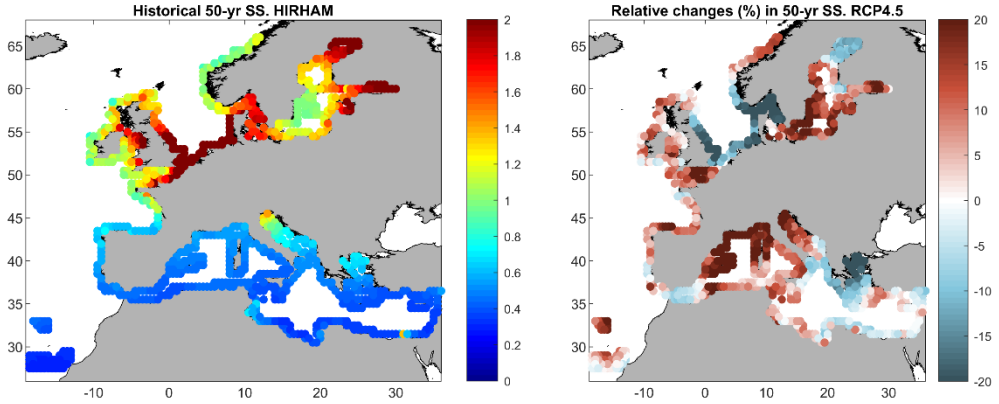

Figure 12. (Left) Historical (1986-2005) extreme storm surge (m) obtained by Muis et al. (2020) in Europe. (Right) Relative future (2081-2100) changes for the RCP4.5 (in percentage).

4.1.8 *Changes in port operability failure due to unfavorable port mouth conditions*

This indicator corresponds with the number of hours per year for which the significant wave height at the port mouth exceeds the threshold of 2.5 m. The historical values of this indicator along the European Atlantic coast and the Western Mediterranean basin exhibits important spatial variations, with values close to 0 along the English Channel, Irish Sea and Canary Islands and higher than 1000 hours/years (up to 2600 hours/year) in the northwest of the Iberian Peninsula and north of UK. Regarding the projected future changes for 2081-2100 period, a decrease is observed in the Mediterranean Sea and an increase in the Atlantic coast (from -272 to 636 hrs/yr and from -374 to 563 hrs/yr for the RCP4.5 and RCP8.5, respectively) (Figure 13). In relative terms, this corresponds to variations between -35% to >100% and between –57% to >100% for both climate scenarios.

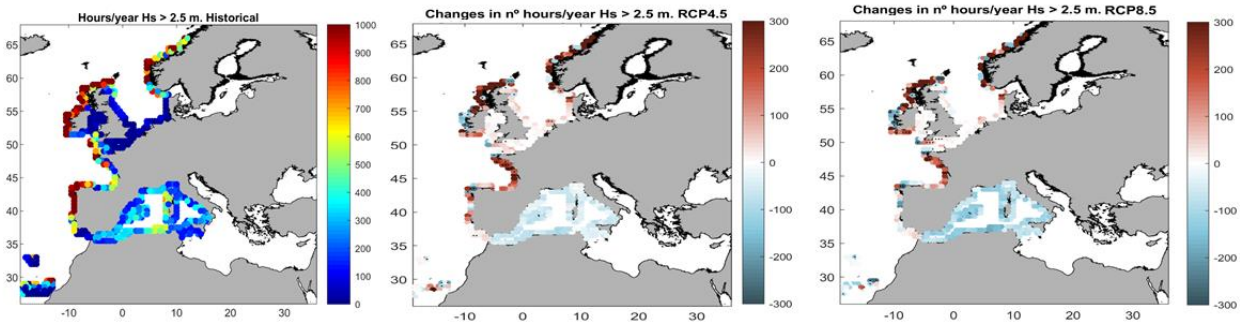

Figure 13. (Left) Historical (1986-2005) unfavorable port mouth wave conditions (i.e. $Hs_{port\ mouth}$ > 2.5 m) (in hours/year) along the Atlantic European coast and Western Mediterranean. Future changes (in hours/year) for the time period 2081-2100, under (center) RCP4.5 and (right) RCP8.5 climate scenarios. Stippling denotes areas where the magnitude of the multi-model ensemble mean exceeds the inter-model standard deviation.

4.1.9 *Changes in port operability failure due to surface agitation*

This indicator corresponds with the number of hours per year for which the significant wave height inside the port exceeds the threshold of 0.4 m. The historical values of this indicator along the European Atlantic coast and the Western Mediterranean basin exhibits important spatial variations, with values close to 0 along the English Channel, Irish Sea and Canary Islands and higher than 1000 hours/years (up to 2286 hours/year) in the northwest of the Iberian Peninsula and north of UK. Regarding the projected future changes for 2081-2100 period, a decrease is observed in the Mediterranean Sea. No significant variations are obtained in the English Channel, Irish Sea and east coast of Great Britain, whereas an increase is expected in the Atlantic coast (from -254 to 637 hrs/yr and from -345 to 562 hrs/yr for the RCP4.5 and RCP8.5, respectively) (Figure 13). In relative terms, this corresponds with variations between -35% to >100% and between –60% to >100% for both climate scenarios.

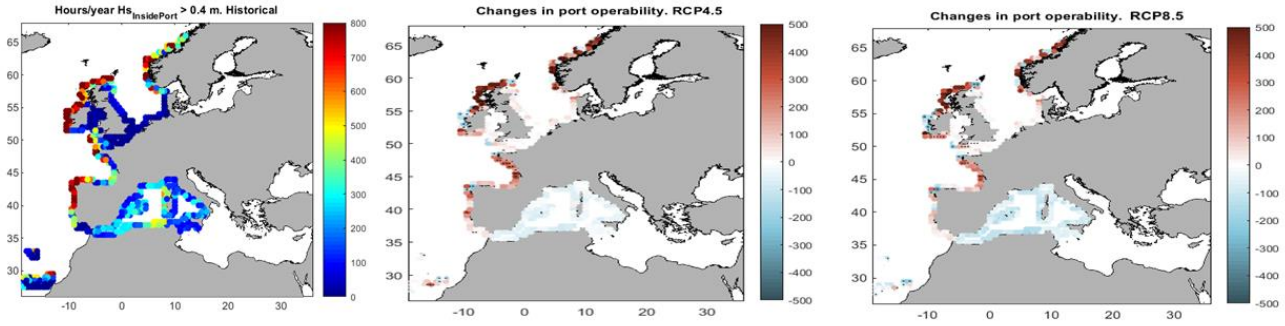

Figure 14. (Left) Historical (1986-2005) wave agitation conditions inside the port (i.e. $Hs_{inside\ port}$ > 0.4 m) (in hours/year) along the Atlantic European coast and Western Mediterranean. Future changes (in hours/year) for the time period 2081-2100, under (center) RCP4.5 and (right) RCP8.5 climate scenarios. Stippling denotes areas where the magnitude of the multi-model ensemble mean exceeds the inter-model standard deviation.

4.1.10 *Changes in coastal flooding at the berth*

This indicator corresponds with the number of hours per year with coastal flooding at the berth. The historical values of this indicator varies from 0.2 hours/year to 1653 hours/year in Southern Europe, with the highest values found in the northwest of the Iberian Peninsula.

The projected future changes for 2081-2100 period show an increase overall, with the maximum rise found at north of Canary Islands. These changes range from 6.8 to 3658 hours/year and from 20.7 to 5720 hours/year for RCP4.5 and RCP8.5, respectively (Figure 15Figure 13).

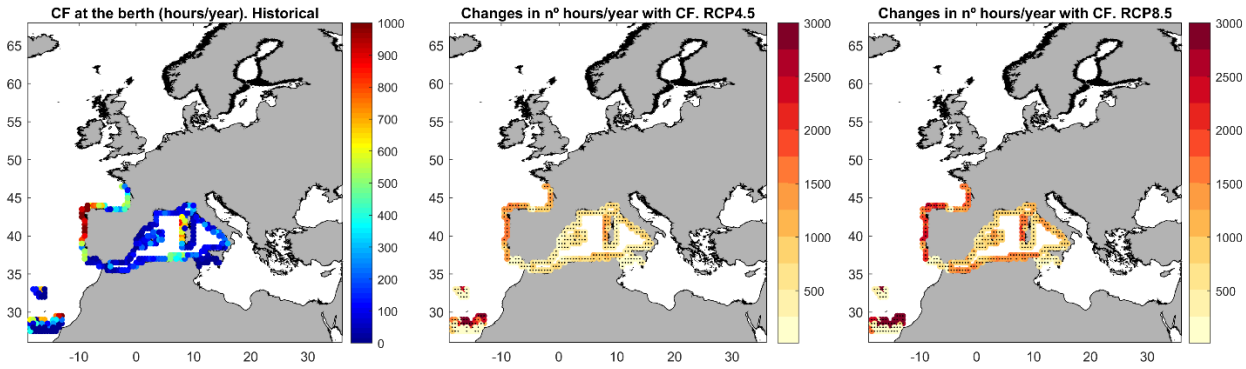

Figure 15. (Left) Historical (1986-2005) frequencies of coastal flooding at the berth (in hours/year) in Southern Europe. Future changes (in hours/year) for the time period 2081-2100, under (center) RCP4.5 and (right) RCP8.5 climate scenarios. Stippling denotes areas where the magnitude of the multi-model ensemble mean exceeds the inter-model standard deviation.

4.1.11 *Changes in wave overtopping conditions for vertical/sloping breakwaters*

This indicator corresponds with the number of hours per year with wave overtopping of vertical and sloping breakwaters. The selected threshold to consider wave overtopping is 0.1 l/m/s. The future changes in this indicator have been evaluated for both kind of breakwaters along the European Atlantic coast and the Western Mediterranean. The historical and future changes values are summarized in Table 3. The highest values for the historical period are found in the NW of the Iberian Peninsula, the north of UK and the Norwegian coast. These values are projected to increase notably in the west coast of France, north of UK and Norway for 2081-2100 period and under both climate scenarios (Figure 16. (Left) Historical (1986-2005) frequencies of wave overtopping for a (top) vertical and (bottom) sloping breakwaters (in hours/year) in Southern Europe. Future changes (in hours/year) for the time period 2081-2100, under (center) RCP4.5 and (right) RCP8.5 climate scenarios for both kind of breakwaters. Stippling denotes areas where the magnitude of the multi-model ensemble mean exceeds the inter-model standard deviation.).

	Historical (hours/year)	Changes for RCP4.5 (hours/year)	Changes for RCP8.5 (hours/year)
Vertical breakwater	0 - 3613	-45 - +978	-44 - +1058
Sloping breakwater	0 - 4303	-65 - +950	-92 - +916

Table 3. Historical frequencies and future changes in wave overtopping for vertical and sloping breakwaters.

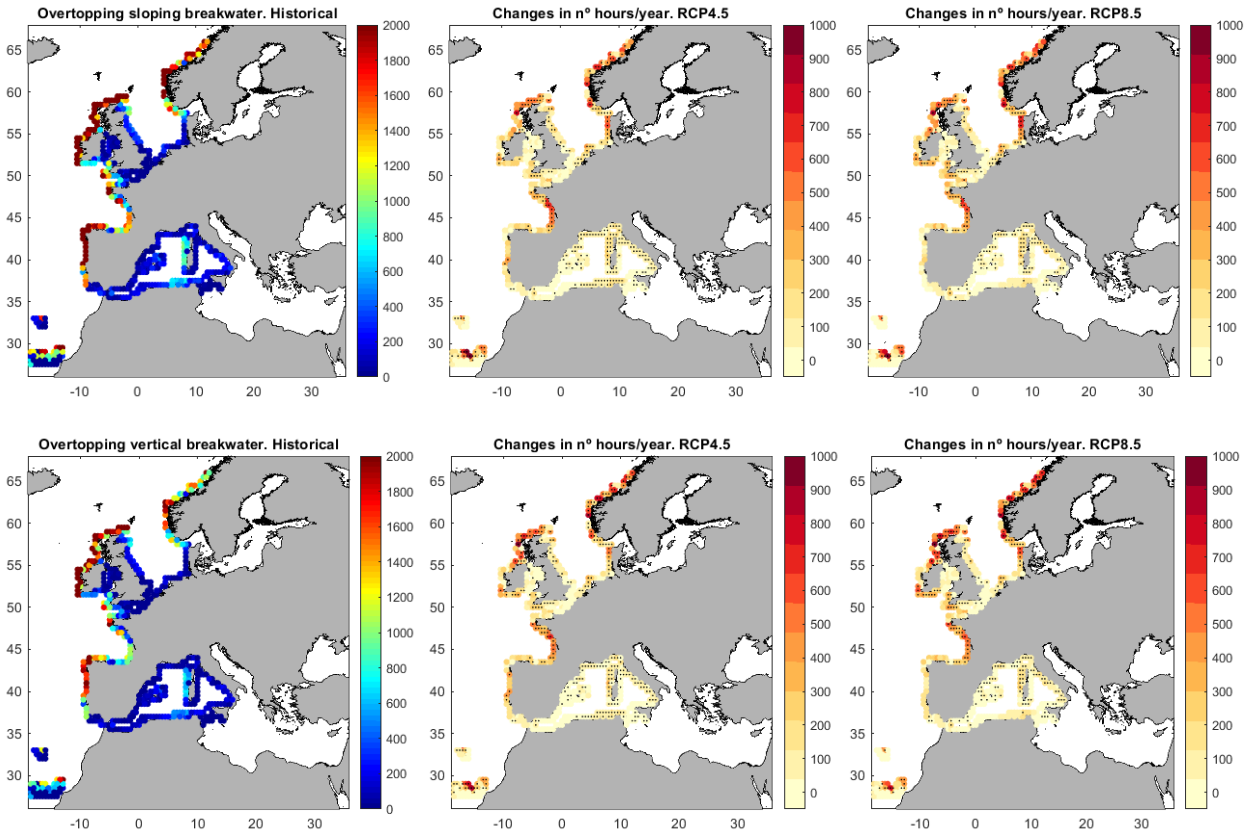

Figure 16. (Left) Historical (1986-2005) frequencies of wave overtopping for a (top) vertical and (bottom) sloping breakwaters (in hours/year) in Southern Europe. Future changes (in hours/year) for the time period 2081-2100, under (center) RCP4.5 and (right) RCP8.5 climate scenarios for both kind of breakwaters. Stippling denotes areas where the magnitude of the multi-model ensemble mean exceeds the inter-model standard deviation.

4.1.12 *Changes in mean Wind speed*

The historical mean surface (10-m) wind speed oscillates between 3.1 and 9.3 m/s in Europe. This indicator is expected to increase in the Baltic and Egeo Seas, to remain with no significant variations along the English Channel and to decrease everywhere else in Europe for the period 2081-2100 and the RCP8.5 scenario. The relative changes range from -8.9% to +4.6% (Figure 17).

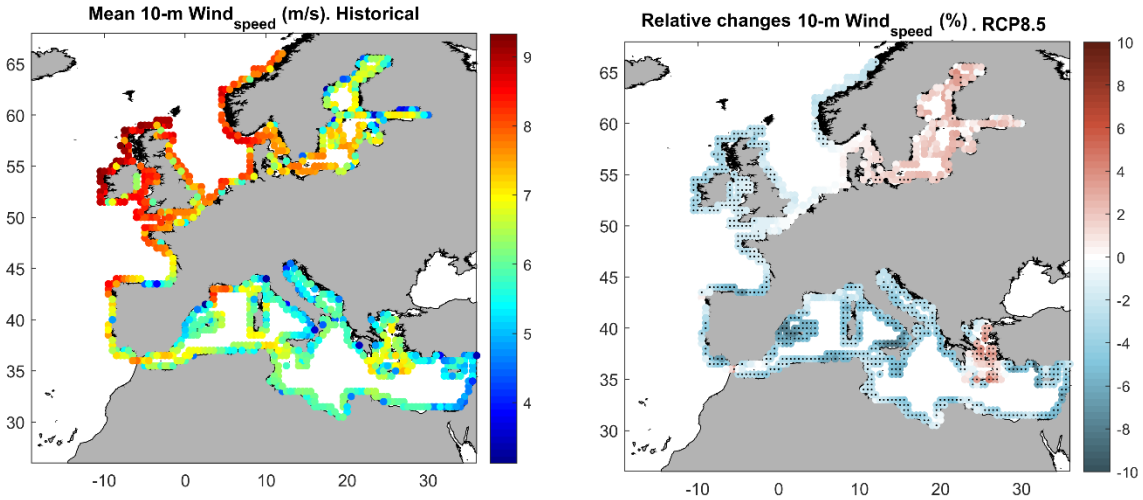

Figure 17. (Left) Historical (1986-2005) mean wind speed at 10 m height in Europe (m/s). (Right) Relative future (2081-2100) changes (in percentage) for the RCP8.5 scenario. Stippling denotes areas where the magnitude of the multi-model ensemble mean exceeds the inter-model standard deviation.

4.1.13 *Changes in mean Wind Power Density*

The historical mean wind power density (WPD) at 100 m height oscillates between 103 and 2204 W/m^2 in Europe. As observed in the previous indicator, the mean WPD is projected to increase in the Baltic and Egeo Seas, to remain with no significant variations along the English Channel and to decrease everywhere else in Europe for the period 2081-2100 and the RCP8.5 scenario. The relative changes range from -23% to +16.16% (Figure 18).

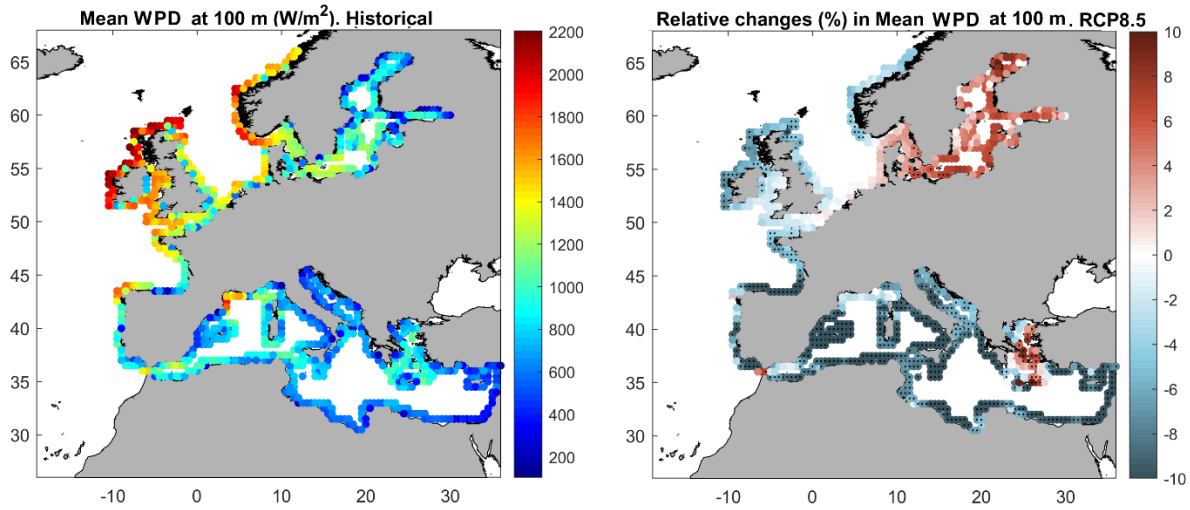

Figure 18. (Left) Historical (1986-2005) mean wind power density at 100 m height in Europe (W/m^2). (Right) Relative future (2081-2100) changes (in percentage) for the RCP8.5 scenario. Stippling denotes areas where the magnitude of the multi-model ensemble mean exceeds the inter-model standard deviation.

4.1.14 *Changes in mean operational Wind time*

The historical mean operational wind time at 100 m height oscillates between 50 and 90% in Europe. Slight future variations in this indicator are expected for the period 2081-2100 and the RCP8.5 scenario, with relative cahnges ranging from -8.5% to +1.85% (Figure 19).

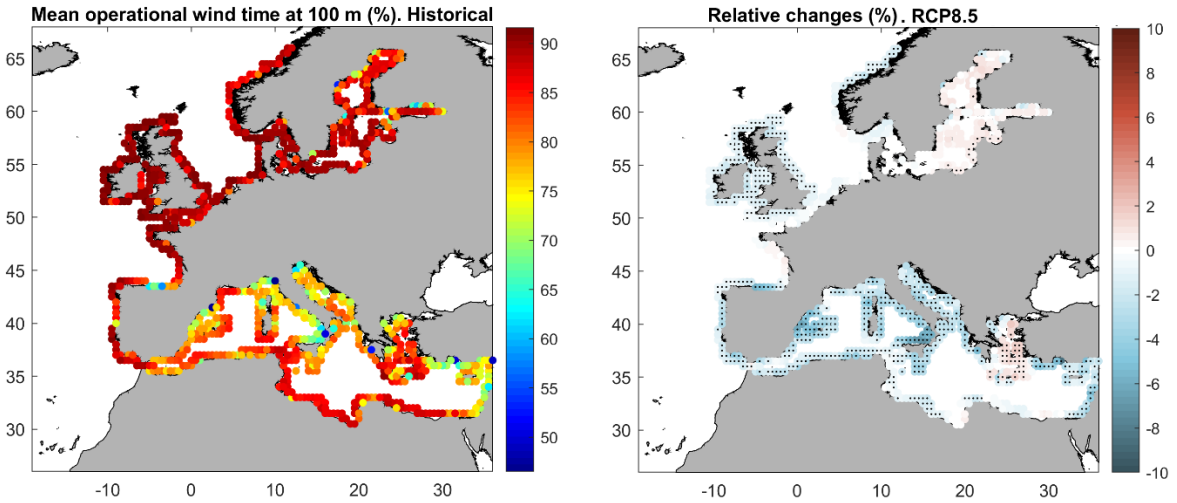

Figure 19. (Left) Historical (1986-2005) mean operational wind time at 100 m height in Europe (in percentage). (Right) Relative future (2081-2100) changes (%) for the RCP8.5 scenario. Stippling denotes areas where the magnitude of the multi-model ensemble mean exceeds the inter-model standard deviation.

4.1.15 *Changes in Extreme Wind Speed*

The historical values in the 10-m wind speed of 50-years return period oscillates between 12.8 m/s and 31.7 m/s in Europe. The future changes in these extreme values show an unclear pattern, but a general decrease is observed in most of the Mediterranean Sea (except at the Egeo Sea). Meanwhile, an increase is expected in most of the Baltic Sea, English Channel, Norwegian coast and Irish Sea. The relative changes range from -10.64% to +9.34% for the future period 2081-2100 and the RCP8.5 scenario (Figure 20).

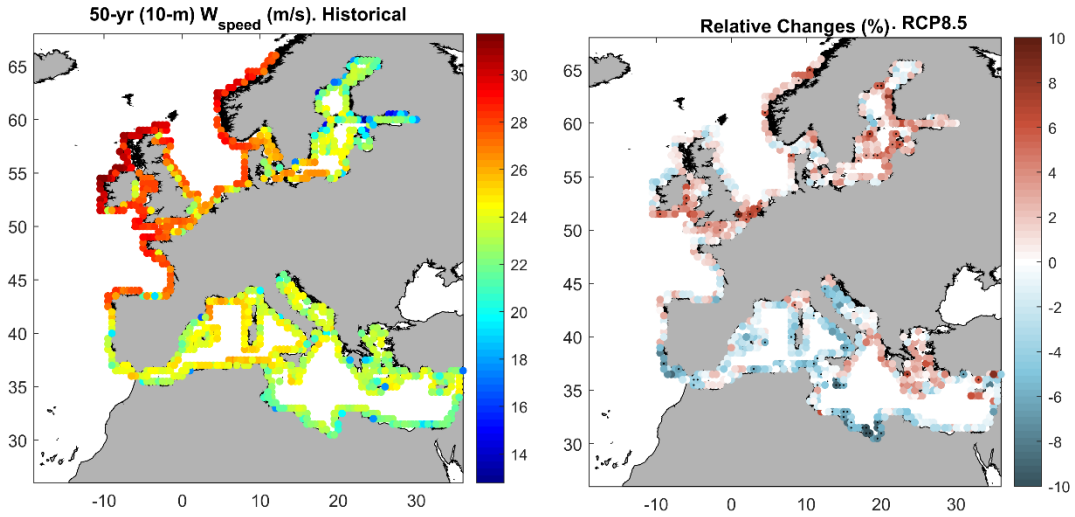

Figure 20. (Left) Historical (1986-2005) 50 years return period (10 m) wind speed in Europe (m/s). (Right) Relative future (2081-2100) changes (in percentage) for the RCP8.5 scenario. Stippling denotes areas where the magnitude of the multi-model ensemble mean exceeds the inter-model standard deviation.

5. References

Airy, G. B. (1845). On tides and waves, Encyclopaedia Metr opolitana, Vol. 5 London: B. Fellowes, 241–396.

Athanasiou, P., van Dongeren, A., Giardino, A., Vousdoukas, M., Gaytan-Aguilar, S., and Ranasinghe, R. (2019). Global distribution of nearshore slopes with implications for coastal retreat, Earth Syst. Sci. Data, 11, 1515–1529, https://doi.org/10.5194/essd-11-1515-2019.

Bruun, P (1962). Sea-Level Rise as a Cause of Shore Erosion. J. Waterw. Harb. Div., 88, 117–132.

Bruun, P (1988). The Bruun Rule of Erosion by Sea-Level Rise: A Discussion on Large-Scale Two- and Three-Dimensional Usages. Journal of Coastal Research. Vol. 4, No. 4.

Dean, R.G. (1976). Beach erosion: causes, processes, and remedial measures Crit. Rev. Environ. Contr., 6 (3), pp. 259-296.

Dean RG. (1977). Equilibrium beach profile: US Atlantic and Gulf Coasts, Department of Civil Engineering. Ocean Engineering Rep. No. 12. University of Delaware, Newark.

Dean, R.G. (1985). Physical modeling of littoral processes. R.A. Dalrymple (Ed.), Physical Modelling in Coastal Engineering, A.A. Balkema, Rotterdam, Boston, pp. 119-139.

Egbert, G.D., & Erofeeva, S.Y., (2002). Efficient inverse modeling of barotropic ocean tides. Journal of Atmospheric and Oceanic Technology 19.2, 183-204.

Franco, L., de Gerloni, M., and van der Meer, J. (1994). Wave overtopping on vertical and composite breakwaters. Coastal Engineering Proceedings, 1(24). https://doi.org/10.9753/icce.v24.

Goda, Y. (1975). Irregular wave deformation in the surf zone. Coastal Engineering in Japan, JSCE 18, 13–26.

Guo, J. (2002). Simple and explicit solution of wave dispersion equation. Coastal Engineering, vol. 45, no 2, pp 71-74.

Hemer, M., Fan, Y., Mori, N., Semedo,A. and Wang, X.L.. (2013). Projected changes in wave climate from a multi-model ensemble. Nature Clim Change 3, 471–476. https://doi.org/10.1038/nclimate1791

Hennessey, J. (1977) 'Some aspects of wind power statistics', Journal of Applied Meteorology, 16(2), pp. 119–128.

Hinton, C., Nicholls, R.J. (1998).Spatial and temporal behaviour of depth of closure along the Holland coast. Proceedings of the Coastal Engineering Conference, 3, pp. 2913-2925.

IPCC (2013), Climate change 2013: The physical science basis, in Contribution of Working Group I to the Fifth Assessment Report of the Intergovernmental Panel on Climate Change, edited by T. F. Stocker, D. Qin, G.-K. Plattner, M. Tignor, S. K. Allen, J. Boschung, A. Nauels, Y.Xia, V. Bex and P. M. Midgley, Intergovern. Panel Clim. Change, Geneva.

Izaguirre, C.; Losada, I.; Camus, P.; Vigh, J. & Stenek, V. (2021). Climate change risk to global port operations. Nature Climate Change. 11. 10.1038/s41558-020-00937-z.

Lobeto, H., Menendez, M. and Losada, I. (2021). Future behavior of wind wave extremes due to climate change. Nature scientific reports 11: 7869. https://doi.org/10.1038/s41598-021-86524-4

Melet, A., Almar, R., Hemer, M., Le Cozannet, G., Meyssignac, B.,and Ruggiero, P. (2020). Contribution of wave setup to projected coastal sea level changes. Journal of Geophysical Research: Oceans, 125, e2020JC016078. https://doi.org/10.1029/2020JC016078.

Meucci, A., Young, I.R., Hemer, M., Kirezci, E., Ranasinghe, R. (2020). Projected 21st century changes in extreme wind-wave events. Sci Adv. 2020 Jun 10;6(24):eaaz7295. doi: 10.1126/sciadv.aaz7295. PMID: 32577512; PMCID: PMC7286683.

Miller, J.K. and Livermont, E. (2008). A predictive index for wave and storm surge induced erosion. Proceedings of the 31st International Conference on Coastal Engineering, Hamburg, Germany.

Muis, S., Apecechea, M.I., Dullaart, J., de Lima, R.J., Madsen, K.S., Su, J., Yan, K., Verlaan, M. (2020), A High-Resolution Global Dataset of Extreme Sea Levels, Tides, and Storm Surges, Including Future Projections.Frontiers in Marine Science, vol 7,263, https://doi.org/10.3389/fmars.2020.00263.

Rueda, A., Vitousek, S., Camus, P., Tomas, A., Espejo, A., Losada, I. J., et al. (2017). Global classification of coastal flooding climates. Scientific Reports, 7(1), 5038. https://doi.org/10.1038/s41598-017-05090-w.

Stockdon, H. F., Holman, R. A., Howd, P. A., & Sallenger, A. H. (2006). Empirical parameterization of setup, swash, and runup. Coastal Engineering, 53(7), 573–588. https://doi.org/10.1016/j.coastaleng.2005.12.005.

Sunamura, T. (1984). Quantitative predictions of beach-face slopes. Geological Society of America Bulletin, 95(2), 242–245. https://doi.org/10.1130/0016-7606(1984)95<242:QPOBS>2.0.CO;2

Thiéblemont, R.; Le Cozannet, G.; Toimil, A.; Meyssignac, B.; Losada, I.J. (2019). Likely and High-End Impacts of Regional Sea-Level Rise on the Shoreline Change of European Sandy Coasts Under a High Greenhouse Gas Emissions Scenario. Water, 11, 2607. https://doi.org/10.3390/w11122607

Vousdoukas, M. I., Mentaschi, L., Voukouvalas, E., Verlaan, M. and Feyen, L. (2017). Extreme sea levels on the rise along Europe's coasts. Earth's Future. https://doi.org/10.1002/2016EF000505.

Vousdoukas, M. I., Ranasinghe, R., Mentaschi, L., Plomaritis, T.A., Athanasiou, P. Luijendijk, A. and Feyen, L. (2020) Sandy coastlines under threat of erosion. Nat. Clim. Change 10, 260–263. https://doi.org/10.1038/s41558-020-0697-0

Wall, J.P. and van der Meer, J.W. (1992). Wave Run-up and Overtopping on Coastal Structures, Chapter 134, Coastal Engineering.